Improved One-Cycle Control Algorithm in Five-Phase Six-Leg Switching Power Amplifiers for Magnetic Suspension Bearing

LIU Chengzi, YAN Ting, YANG Yan, LIU Zeyuan*

College of Automation & College of Artificial Intelligence, Nanjing University of Posts and Telecommunications, Nanjing 210023, P. R. China

(Received 15 May 2020; revised 20 July 2020; accepted 25 July 2020)

Abstract: For the advantages of easy realization and rapidly intelligent response, the one-cycle control was applied in five-phase six-leg switching power amplifier for magnetic bearing. This paper improves the one-cycle control considering resistance voltage drop and derives its mathematical models. The improved algorithm is compared with the former one. The simulation and experimental results show that the improved algorithm can effectively reduce the output current ripple, achieve good tracking of the given current, improve the control accuracy, and verify the effectiveness and superiority of the method.

Key words: one-cycle control; magnetic bearing; switching power amplifier; voltage drop

CLC number: TM3 **Document code:** A **Article ID:** 1005-1120(2020)05-0796-08

0 Introduction

Owing to the advantages of no friction-loss, low noise and long life, the magnetic bearing has wide application prospects in flywheel energy storage, high-speed machine tools and other fields[1-4]. As a key part of magnetic suspension system, the control accuracy of power amplifier directly affects the levitation performance of magnetic bearing. At present, the permanent magnet biased magnetic bearing[5] requires power amplifier to provide bi-directional current, which usually uses the H-bridge structure as its power topology. In the magnetic bearing systems of multiple degrees-of-freedom (DOFs), the multiple H-bridges structure[6-7] is commonly used, which takes the larger bulk and increases the complicacy and cost of the system. And the introduction of multi-leg switching power amplifier (SPA) topology[8-10] reduces the bulk and the cost of SPA. Li[11] proposed the topology of five-phase six-leg SPA (FPSL-SPA), which reduced the power switch amount by 40% compared to five-H-bridge power amplifiers.

At present, there are many kinds of control strategies in the research of multi-leg SPA of magnetic bearing. Some research used the space vector pulse width modulation (SVPWM)[12-14] to control the topology. However, the control algorithm was complex and had high demand for the controller. Li et al.[15] proposed proportion-integral-derivative (PID) regulator to control the topology of multi-leg SPA. Due to the existence of neutral leg, the control of 5-DOF was easy to be coupled, which was difficult to implement the decoupled control. In addition, the existing maximum current error method, sampling and holding method, node potential method, hysteresis control method and other control strategies[16-17] also have the problem of output coupling. Some scholars[18-19] studied the control of neutral legs in multi-leg structure, which reduced the coupling between each leg to some extent, but the coupled was still strong. Liu et al.[20] proposed the application of one-cycle control (OCC) in the topology of FPSL-SPA. The algorithm had the advantag-

*Corresponding author, E-mail address: liuchengzi@njupt.edu.cn.

How to cite this article: LIU Chengzi, YAN Ting, YANG Yan, et al. Improved one-cycle control algorithm in five-phase six-leg switching power amplifiers for magnetic suspension bearing[J]. Transactions of Nanjing University of Aeronautics and Astronautics, 2020, 37(5): 796-803.

http://dx.doi.org/10.16356/j.1005-1120.2020.05.014

es of simple control, small computation, fast response, high control precision and versatility, and obtained control effects. At the same time, the coupling between 5-DOF was eliminated by fixing duty cycle of the neural leg for enabling separate control of each phase. However, there is little research on OCC of FPSL-SPA, and it is still in the basic research stage. In the process of deriving the mathematical model of OCC, the voltage drop caused by the coil resistance of magnetic bearing is ignored[20]. Therefore, the established model is not accurate enough to track the current accurately.

This paper aims at the above problems and improves the unipolar and bipolar OCC algorithm[20] considering the coil resistance voltage drop. The mathematic model of this algorithm is constructed and the implementation process is designed. The algorithms before and after improvement are compared, and emulational and experimental results are given out to verify the effectiveness of the algorithm.

1 Principle of FPSL-SPA

The topology of FPSL-SPA is shown in Fig.1, constituted by twelve switches and one DC voltage source, and M with different subscripts is signals of different switches. In SPA, legs of phases A—E are loaded, the leg of phase N is neutral, and L_a—L_e are five inductive loads, which are connected to the loaded legs and the neutral leg. In order to achieve independent control of each phase current, the duty cycle of neutral leg is fixed as 0.5[20].

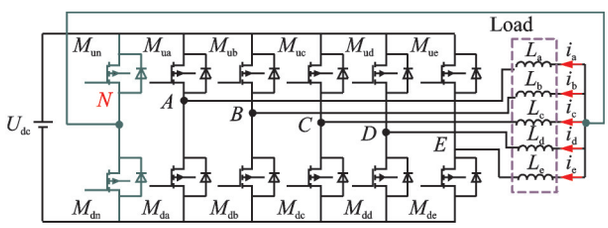

Fig.1 Five-phase six-leg switching power amplifier

The control schematic diagram of single DOF SPA system for magnetic bearing is shown in Fig.2. It is composed of controller, switching power amplifier and current sensor.

The controller is made up of digital signal processing (DSP), which is the main control chip. According to the principle of OCC, the duty cycle of each switch is calculated and the corresponding switching signal is generated. SPA is the main circuit, which realizes the dynamic control of coil current of magnetic bearing, and the current sensor is responsible for detecting the real-time current of coil.

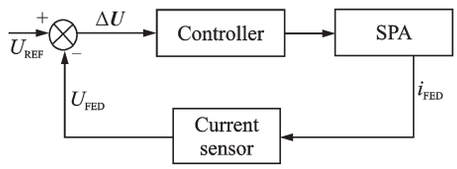

Fig.2 Control diagram of single degree of freedom SPA

When the duty cycle of neutral leg is fixed as a constant, the operation process of each phase is similar, and here we discuss the operation process of loaded phase A.

Fig.3 shows the circuit of the loaded phase A and the neutral leg. To facilitate description, switching function S_a and S_n are introduced as

$$S_a = \begin{cases} 1 & M_{ua} \text{ is on and } M_{da} \text{ is off} \\ 0 & M_{ua} \text{ is off and } M_{da} \text{ is on} \end{cases} \tag{1}$$

$$S_n = \begin{cases} 1 & M_{un} \text{ is on and } M_{dn} \text{ is off} \\ 0 & M_{un} \text{ is off and } M_{dn} \text{ is on} \end{cases} \tag{2}$$

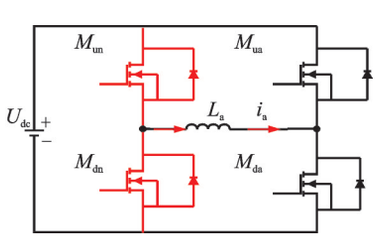

Fig.3 Equivalent circuit of the loaded phase A and neutral leg

According to the condition of switches, there are four working states of phase A as follows:

(1) When $S_a = 0$ and $S_n = 0$, the coil of phase A is in the continuous current state;

(2) When $S_a = 0$ and $S_n = 1$, the coil of phase A is in the adverse charging state;

(3) When $S_a = 1$ and $S_n = 0$, the coil of phase A is in the forward charging state;

(4) When $S_a = 1$ and $S_n = 1$, the coil of phase A is in the continuous current state.

From the above analysis, it can be seen that

when the OCC of FPSL-SPA works, the phase A converts among four working states and enables the coil current of magnetic bearing to follow the change of the given signal.

2 Improvement of One-Cycle Control Method

According to the different switching status, OCC can be divided into unipolar OCC and bipolar OCC[20], and the control process of the two OCCs is quite different. Using the unipolar OCC, the charging and discharging status of the one DOF magnetic bearing coil do not exist simultaneously in one switching cycle, but the phenomenon exists in the bipolar OCC. This paper optimizes the mathematical model of unipolar and bipolar OCC algorithm considering the influence of coil resistance R of magnetic bearing, and comparatively analyzes the OCC algorithm before and after improvement. Because the measured conduction voltage drop of the switch is small, it is neglected in the analysis process.

2.1 Improvement of bipolar OCC algorithm

The upper and lower switches of the same leg are complementarily conducted by the bipolar OCC. The duty cycle of the upper switch of the loaded leg is calculated by the OCC algorithm. Pulse width modulation (PWM) waveform generation mode and the corresponding current variation are shown in Fig.4, where M_{ua} is the signal of the upper switch of loaded leg of phase A, M_{un} the signal of the upper switch of the neutral leg, PRD the value of the time reference period register in DSP, D_a the duty cycle of M_{ua}, and D_n the duty cycle of M_{un}. From Fig.4, we can see that:

(1) During the periods from t_0 to t_1 and from t_4 to t_5, the voltages at both ends of the coil are U_{dc}, and the current is in charging state and keeps rising. It can be expressed as

$$L\frac{\mathrm{d}i}{\mathrm{d}t}+iR=U_{dc} \tag{3}$$

where L is the coil inductance, R the coil resistance, and i the coil current.

(2) During the periods from t_1 to t_2 and from t_3 to t_4, the voltages at both ends of the coil are zero, and the current is in the continuous state and keeps decreasing slowly. It can be expressed as

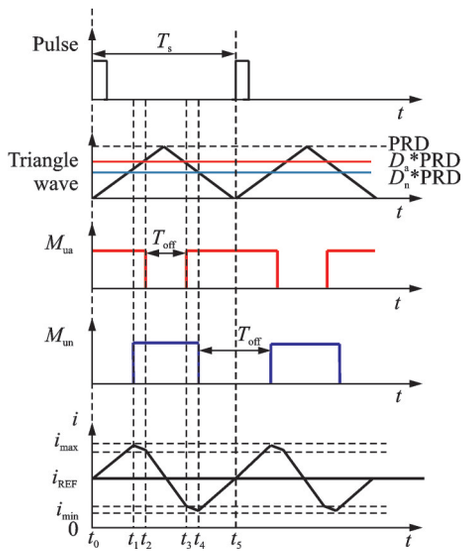

Fig.4 Waveforms of bipolar OCC

$$L\frac{\mathrm{d}i}{\mathrm{d}t}+iR=0 \tag{4}$$

(3) During the period from t_2 to t_3, the voltages at both ends of the coil are $-U_{dc}$, which is in the state of discharging, and the current decreases. In this case, it can be expressed as

$$L\frac{\mathrm{d}i}{\mathrm{d}t}+iR=-U_{dc} \tag{5}$$

According to Eqs.(3)—(5), we can derive that

$$\begin{aligned}
&i(t)=\frac{U_{dc}}{R}+\left[i(t_0)-\frac{U_{dc}}{R}\right]\mathrm{e}^{-R(t-t_0)/L} && {}_0\leqslant t\leqslant t_1\\
&i(t)=i(t_1)\mathrm{e}^{-R(t-t_1)/L} && t_1\leqslant t\leqslant t_2\\
&i(t)=-\frac{U_{dc}}{R}+\left[i(t_2)+\frac{U_{dc}}{R}\right]\mathrm{e}^{-R(t-t_2)/L} && t_2\leqslant t\leqslant t_3\\
&i(t)=i(t_3)\mathrm{e}^{-R(t-t_3)/L} && t_3\leqslant t\leqslant t_4\\
&i(t)=\frac{U_{dc}}{R}+\left[i(t_4)-\frac{U_{dc}}{R}\right]\mathrm{e}^{-R(t-t_4)/L} && t_4\leqslant t\leqslant t_5
\end{aligned} \tag{6}$$

Thus, the value of current at the end of one cycle can be obtained that

$$i(t_5)\approx\frac{U_{dc}}{L}[(t_5-t_4)-(t_3-t_2)+(t_1-t_0)]+i(t_0)\mathrm{e}^{-RT_s/L} \tag{7}$$

Also it can be seen from Fig.4 that

$$\begin{aligned}
t_5-t_4&=t_1-t_0=\frac{T_s}{4}\\
t_3-t_2&=(1-D)T_s
\end{aligned} \tag{8}$$

Therefore, we have

$$i(t_5)\approx\frac{U_{dc}T_s}{L}\left(D-\frac{1}{2}\right)+[\,i_{REF}-\Delta i(n)\,]\,e^{-RT_s/L} \quad (9)$$

where T_s is the switching cycle and D the duty cycle of loaded leg. So, in order to make the current keep up with the given value in one cycle, it should be

$$i(t_5)=i_{REF} \quad (10)$$

Then there is

$$i_{REF}\approx\frac{U_{dc}T_s}{L}\left(D-\frac{1}{2}\right)+[\,i_{REF}-\Delta i(n)\,]\,e^{-RT_s/L} \quad (11)$$

where i_{REF} is the given value of current and $\Delta i(n)$ the deviation between the given current and the actual current at t_0 moment.

Therefore, in order to ensure that the current follows the given value within one cycle under the bipolar OCC, the duty cycle of switch M_{ua} can be expressed as

$$D=\frac{i_{REF}(1-e^{-RT_s/L})L}{U_{dc}T_s}+\frac{\Delta i(n)e^{-RT_s/L}}{U_{dc}T_s}+\frac{1}{2} \quad (12)$$

According to Eq.(12), the improved bipolar OCC algorithm is proposed.

Because the influence of coil resistance is neglected when deriving the mathematical model of bipolar OCC[20], the model is not accurate enough. The duty cycle of switch M_{ua} before improvement of bipolar OCC can be expressed as

$$D'=\frac{\Delta i(n)L}{U_{dc}T_s}+\frac{1}{2} \quad (13)$$

By substituting Eq.(13) into Eq.(9) and using the control algorithm before improvement, the current at the end of the cycle can be obtained as

$$i(t_5)'\approx\Delta i(n)+[\,i_{REF}-\Delta i(n)\,]\,e^{-RT_s/L} \quad (14)$$

It can be seen that when the influence of coil resistance is taken into account, there is still a deviation between the current obtained by the original OCC algorithm and the given one at the end of the switching cycle, and then the deviation of the current can be expressed as

$$\Delta i(n+1)'=i_{REF}-i(t_5)'=[\,i_{REF}-\Delta i(n)\,][1-e^{-RT_s/L}]\approx i_{REF}[1-e^{-RT_s/L}] \quad (15)$$

2.2 Improvement of unipolar OCC algorithm

Different from the bipolar OCC algorithm, the unipolar OCC algorithm changes the switching sequence of the upper and lower switches of the neutral leg, and the control result is also different from that of the bipolar OCC algorithm. The PWM generation mode and current waveforms of unipolar OCC are shown in Fig.5.

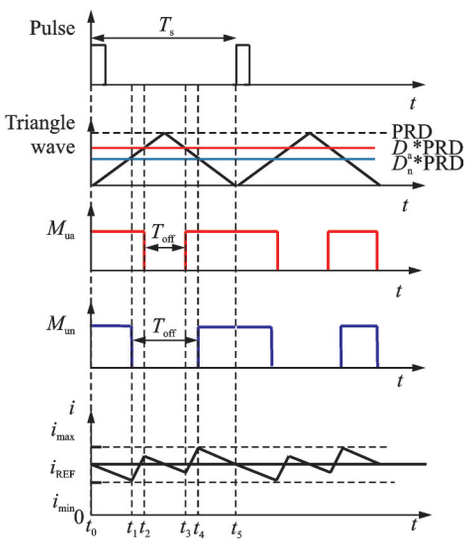

Fig.5 Waveforms of unipolar OCC

(1) During the periods from t_1 to t_2 and from t_3 to t_4, the voltages at both ends of the coil are U_{dc}, and the current is in charging state and keeps rising. It can be expressed as

$$L\frac{di}{dt}+iR=U_{dc} \quad (16)$$

(2) During the periods from t_0 to t_1, from t_2 to t_3 and from t_4 to t_5, the voltages at both ends of the coil are zero, and the current is in the continuous state and keeps decreasing slowly. It can be expressed as

$$L\frac{di}{dt}+iR=0 \quad (17)$$

According to Eqs.(16) and (17), we can derive that

$$\begin{aligned}
&i(t)=i(t_0)e^{-R(t-t_0)/L} && t_0\leqslant t\leqslant t_1\\
&i(t)=\frac{U_{dc}}{R}+\left[i(t_1)-\frac{U_{dc}}{R}\right]e^{-R(t-t_1)/L} && t_1\leqslant t\leqslant t_2\\
&i(t)=i(t_2)e^{-R(t-t_2)/L} && t_2\leqslant t\leqslant t_3\\
&i(t)=\frac{U_{dc}}{R}+\left[i(t_3)-\frac{U_{dc}}{R}\right]e^{-R(t-t_3)/L} && t_3\leqslant t\leqslant t_4\\
&i(t)=i(t_4)e^{-R(t-t_4)/L} && t_4\leqslant t\leqslant t_5
\end{aligned} \quad (18)$$

Thus, the current at the end of one cycle can be obtained as

$$i(t_5)\approx \frac{U_{dc}}{L}\left[(t_4-t_3)+(t_2-t_1)\right]+i(t_0)e^{-RT_s/L} \quad (19)$$

Also it can be seen from Fig.5 that

$$t_4-t_3=t_2-t_1=\left(\frac{D}{2}-\frac{1}{4}\right)T_s \quad (20)$$

By substituting Eq.(20) into Eq.(19), we can obtain that

$$i(t_5)\approx \frac{U_{dc}T_s}{L}\left(D-\frac{1}{2}\right)+\left[i_{REF}-\Delta i(n)\right]e^{-RT_s/L} \quad (21)$$

In order to make the current keep up with the given value, it should be

$$i(t_5)=i_{REF} \quad (22)$$

Then there is

$$i_{REF}\approx \frac{U_{dc}T_s}{L}\left(D-\frac{1}{2}\right)+\left[i_{REF}-\Delta i(n)\right]e^{-RT_s/L} \quad (23)$$

Therefore, in order to ensure that the current follows the given value in one cycle using unipolar OCC, the duty cycle of switch M_{ua} can be obtained as

$$D=\frac{i_{REF}(1-e^{-RT_s/L})L}{U_{dc}T_s}+\frac{\Delta i(n)e^{-RT_s/L}L}{U_{dc}T_s}+\frac{1}{2} \quad (24)$$

According to Eq.(24), the improved unipolar OCC algorithm is proposed.

However, by the unipolar OCC algorithm before improvement, the duty cycle of switch M_{ua} can be obtained as[20]

$$D'=\frac{\Delta i(n)L}{U_{dc}T_s}+\frac{1}{2} \quad (25)$$

By substituting Eq.(25) into Eq.(21), the current at the end of a period can be obtained as

$$i(t_5)'\approx \Delta i(n)+\left[i_{REF}-\Delta i(n)\right]e^{-RT_s/L} \quad (26)$$

Therefore, there is still deviation between the current obtained by unipolar OCC algorithm before improvement and the given one at the end of the switching cycle, and then the deviation of the current can be expressed as

$$\Delta i(n+1)'=i_{REF}-i(t_5)'=\left[i_{REF}-\Delta i(n)\right]\left[1-e^{-RT_s/L}\right]\approx i_{REF}\left[1-e^{-RT_s/L}\right] \quad (27)$$

3 Simulation and Experiment

In order to verify the feasibility and superiority of the mathematical models of the two improved OCC algorithms, this paper builds a simulation model with MATLAB and carries out the experimental verification. In the simulation and experiments, the inductance coil is used as a load, which includes L = 3.5 mH and R= 1.0 Ω. Both simulation and experimental conditions are set as: bus voltage U_{dc}=20 V and switching frequency f_s= 40 kHz.

3.1 Simulation and experiment of bipolar OCC

Fig.6(a) is the simulation result of the improved bipolar OCC for the input of sinusoidal wave with frequency of 400 Hz and amplitude of 0.8 V, which shows the output current tracking effect is good. In order to comparatively analyze the algorithm before and after improvement, simulation and experiment are carried out under the given current i_{REF}=1.2 A. Fig.6(b) is the simulation waveform of the algorithm before improvement. It can be seen that there is a deviation between the average tracking current and the given value. Therefore, the tracking is not accurate. Compared with the original algorithm, the improved algorithm considers the influence of the resistance voltage drop of the magnetic bearing coil on the current, so the mathematical model is more accurate. The simulation waveform of the improved bipolar OCC is shown in Fig.6(c). It can be seen that the average tracking current of the improved algorithm is almost unbiased with the given one, which verifies the effectiveness of the improved algorithm.

Fig.7(a) is the corresponding experimental waveform. From the simulation and experimental results, it can be seen that the improved algorithm can track the current well, and the feasibility of the improved bipolar OCC algorithm is verified. The experimental results of Fig. 7(b) and Fig. 7(c) also prove the superiority of the improved bipolar OCC algorithm.

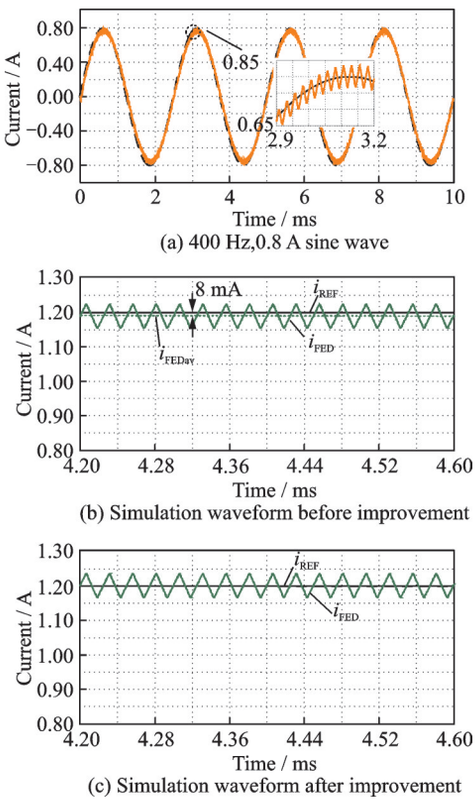

(a) 400 Hz,0.8 A sine wave

(b) Simulation waveform before improvement

(c) Simulation waveform after improvement

Fig.6 Simulation waveforms of bipolar OCC

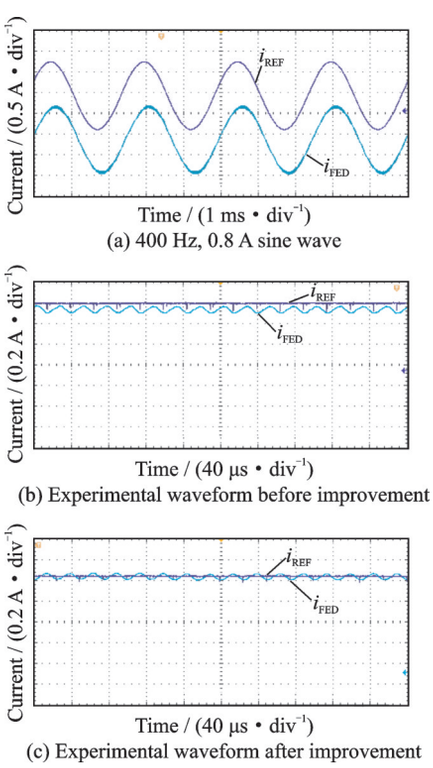

(a) 400 Hz, 0.8 A sine wave

(b) Experimental waveform before improvement

(c) Experimental waveform after improvement

Fig.7 Experimental waveforms of bipolar OCC

3.2 Simulation and experiment of unipolar OCC

Similar to the bipolar OCC, simulation and experiment of unipolar OCC are carried out, and waveforms are shown in Fig.8 and Fig.9, respectively. From Fig.8(a) and Fig.9(a), it can be seen that the improved algorithm can track the current well, which verifies the feasibility of the improved unipolar OCC algorithm. As can be seen from Fig.8(b), there is a deviation between the average tracking current and the given value when using the algorithm before improvement, and the tracking is not accurate. By comparing simulation results in Figs.8(b) and(c), it can be seen that the tracking waveform of the improved algorithm is more accurate than that before improvement, which verifies the effectiveness of the improved algorithm in this paper. The experimental results in Figs.9(b) and(c) also can prove the superiority of the improved unipolar OCC algorithm.

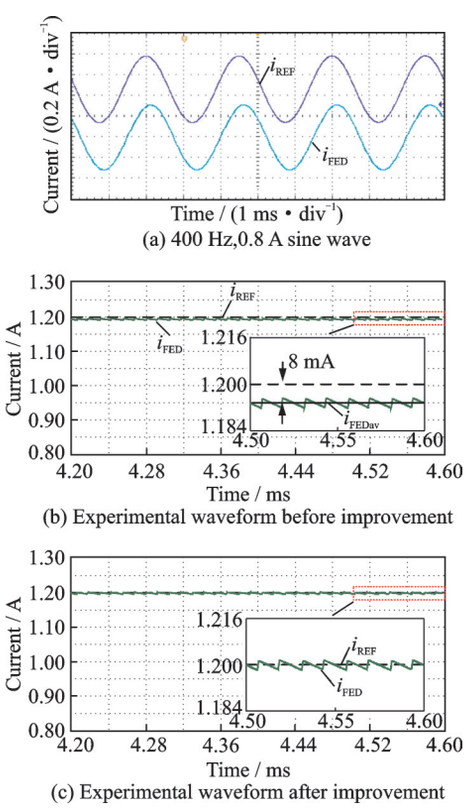

(a) 400 Hz,0.8 A sine wave

(b) Experimental waveform before improvement

(c) Experimental waveform after improvement

Fig.8 Simulation waveforms of unipolar OCC

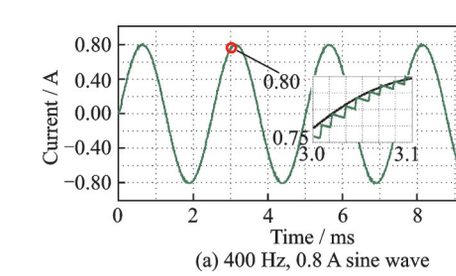

(a) 400 Hz, 0.8 A sine wave

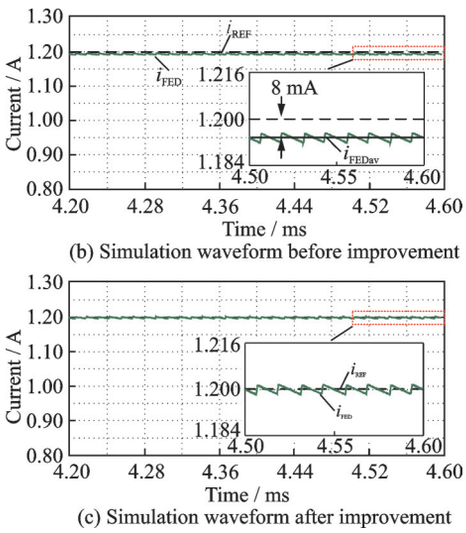

Fig.9 Experimental waveforms of unipolar OCC

4 Conclusions

Considering the coil resistance voltage drop, this paper improves the unipolar OCC algorithm and the bipolar OCC algorithm, and optimizes the mathematical models of the two OCC algorithms. The theory, simulation and experiment show that the mathematical model of the improved algorithm is more accurate and the control effect is better than that before improvement. It is helpful to improve the control accuracy of the one-circle control algorithm in the FPSL-SPA of magnetic suspension bearing.

References

[1] DU T, GENG H, SUN Y, et al. Theoretical and experimental researches of active magnetic bearing systems for high-speed PM machines[J]. Int J Appl Electromagnet Mech, 2019, 59(3): 891-901.

[2] DENK J. Active magnetic bearing technology running successfully in Europe's biggest onshore gas field[J]. Oil Gas Eur Mag, 2015, 41(2): 91-92.

[3] WANG Xiaolin, DENG Zhiquan, YAN Yangguang. Innovative motor with five-degree magnetic suspension [J]. Journal of Nanjing University of Aeronautics & Astronautics, 2004, 36(2): 210-214. (in Chinese)

[4] CAO Xin, CHEN Huateng, DENG Zhiquan. Analogy study of two types of multi-degree-of-freedom switched reluctance motors[J]. Journal of Nanjing University of Aeronautics & Astronautics, 2020, 52 (2): 171-180. (in Chinese)

[5] ZHAO X S, DENG Z Q, WANG X L, et al. Research status and development of permanent magnet biased magnetic bearings[J]. Transactions of China Electrotechnical Society, 2009, 24(9): 9-20.

[6] FEI Q Z, DENG Z Q, WANG X L, et al. A control strategy of novel five-phase six-leg switching power amplifiers applied in magnetic levitating bearing systems[J]. Proc Chin Soc Elect Eng, 2012, 32(9): 124-131.

[7] WANG J, XU L X. Equivalent mathematical model of switching power amplifier for magnetic bearing[J]. Transactions of China Electrotechnical Society, 2010, 25(4): 53-58.

[8] JAHNS T M, DE D R, RADUN A V, et al. System design considerations for a high-power aerospace resonant link converter[C]//Proceedings of IEEE Appl Power Electron. Boston, MA, United States: IEEE, 1992: 665-673.

[9] LIU C Z, DENG Z Q, XIE L, et al. The design of the simple structure-specified controller of magnetic bearings for the high-speed SRM[J]. IEEE ASME Trans Mechatro, 2015, 20(4): 1798-1808.

[10] LIU C Z, DENG Z Q, CAO X, et al. Control strategy of fourth leg in four-leg inverter[J]. Proc Chin Soc Elect Eng, 2015, 35(22): 5899-5907.

[11] LI X S. Research on modulation technologies of multi-leg switching power amplifiers for magnetic Bearing[D]. Nanjing: Nanjing University of Aeronautics and Astronautics, 2010.(in Chinese)

[12] TIAN X, FANG J, LIU G. Magnetic bearing switching power amplifier based on SVPWM control[J]. Syst Eng Electron, 2008, 30(8): 1598-1602.

[13] LI R, SUN Y, QIU H, et al. A control method of switching power amplifiers with triple-arm SVPWM[J]. Hsi An Chiao Tung Ta Hsueh, 2015, 49 (12): 71-76.

[14] LI A, JIANG D, KONG W, et al. A high performance five-phase six-leg VSI and the corresponding SVPWM strategy[C]//Proceedings of IEEE Appl Power Electron. Anaheim, CA, United States: IEEE, 2019: 2538-2543.

[15] LI X S, DENG Z Q, CHEN Z D, et al. A control method of current mode four-leg switching power amplifier[J]. Transactions of China Electrotechnical Society, 2011, 26(2): 156-164.

[16] RUAN X, YAN Y. The control strategy for three-phase inverter with four bridge legs[J]. Transactions of China Electrotechnical Society, 2000, 15(1): 61-64.

[17] HANG L, LI B, ZHANG M, et al. Equivalence of

SVM and carrier-based PWM in three-phase/wire/level Vienna rectifier and capability of unbalanced-load control[J]. IEEE Trans Ind Electron, 2014, 61(1): 20-28.

[18] LIU X, ZHANG H, CHEN H. Control strategy of fourth leg in four-leg inverter[J]. Proc Chin Soc Elect Eng, 2007, 27(33): 87-92.

[19] LIU C Z, DENG Z Q, HUA C, et al. Design and implementation of a five-phase six-leg switching power amplifier for five degrees of freedom magnetic levitation bearing system[C]//Proceedings of IEEE Conf Ind Electron Appl Melbourne. VIC, Australia: IEEE, 2013: 1254-1258.

[20] LIU C Z, DENG Z Q, LI X S, et al. One-cycle decoupling control method of multi-leg switching power amplifier for magnetic bearing system[J]. IET Electr Power Appl, 2019, 13(8): 1204-1211.

Acknowledgement This work was supported by the National Science Foundation of China (No. 51607096).

Author Dr. **LIU Chengzi** received the B. S. and Ph. D. degrees in electrical engineering from Nanjing University of Aeronautics and Astronautics (NUAA) in 2006 and 2015, respectively. In 2015, she joined the Department of Electrical Engineering, Nanjing University of Posts and Telecommunications (NJUPT). Her current research interests include power electronics and magnetic bearing system.

Author contributions Dr. **LIU Chengzi** designed the study, revised and modified the manuscript. Ms. **YAN Ting** conducted the experimental analysis and wrote the manuscript. Dr. **YANG Yan** completed the modeling of the algorithm. Dr. **LIU Zeyuan** made a simulation analysis. All authors commented on the manuscript draft and approved the submission.

Competing interests The authors declare no competing interests.

(Production Editor: ZHANG Huangqun)

磁悬浮轴承五相六桥臂开关功放的单周期控制算法改进

刘程子，严　婷，杨　艳，刘泽远

(南京邮电大学自动化学院/人工智能学院，南京 210023，中国)

摘要：将单周期控制算法应用于磁悬浮轴承五相六桥臂开关功放系统中，具有易于实现和智能响应快的突出优点。本文考虑磁悬浮轴承中线圈电阻压降的影响，对单周期控制算法进行改进，推导出改进后算法的数学模型。将改进后的算法与改进前的算法进行比较。仿真与实验的结果表明，改进后的算法能有效降低输出电流的纹波，实现对给定电流的良好跟踪，提高了控制精度，验证了该方法的有效性和优越性。

关键词：单周期控制；磁悬浮轴承；开关功放；电压降落